



## Research article

# Optimization using central composite design for continuous absorption of CO<sub>2</sub> gas with green sodium silicate in a packed bed column

Dalia Amer Ali<sup>\*</sup>, Mohamed Essam Ibrahim*Department of Chemical Engineering, The British University in Egypt, El-Sherouk City, 11837, Egypt*

## ARTICLE INFO

**Keywords:**

Chemical absorption  
CO<sub>2</sub> gas  
Silica  
Sugarcane bagasse  
Packed bed column  
Optimization

## ABSTRACT

If absolutely nothing is taken to reduce carbon dioxide (CO<sub>2</sub>) emissions, atmospheric concentrations of carbon dioxide will rise to 550 parts per million by 2050, which will have disastrous effects on the world's climate and food production. An apparatus has been designed and setup to convert CO<sub>2</sub> into a useful and vital product which was silica. The effect of different experimental factors on the compositions by weight percent of SiO<sub>2</sub> and Na<sub>2</sub>CO<sub>3</sub> were studied including the CO<sub>2</sub> gas flow rate (1.037, 1.648 and 2.26 L/min), initial concentration of sodium silicate (Na<sub>2</sub>SiO<sub>3</sub>) solution (5, 7.5 and 10 %wt) and the packing size (15.95, 20.175, and 24.4 mm). An optimization process was performed using the Design Expert software program to achieve the optimum experimental conditions at which the maximum weight percent of SiO<sub>2</sub> (main product), the minimum weight percent of (Na<sub>2</sub>CO<sub>3</sub>) (side product) and the minimum reaction time were determined. From the optimization process, the maximum weight percent of SiO<sub>2</sub> (25.63 %), the minimum weight percent of (Na<sub>2</sub>CO<sub>3</sub>) (9.62 %) and the minimum reaction time (7.59 min) were achieved at the following optimum experimental conditions of CO<sub>2</sub> gas flow rate = 1.648 L/min, packing size = 24.4 mm and initial concentration of sodium silicate solution = 10 %wt.

## 1. Introduction

Three-quarters of all emissions come from carbon dioxide, making it the principal greenhouse gas [1]. Carbon dioxide, the most harmful and pervasive greenhouse gas, is now reaching record highs in the atmosphere [2,3]. It is mostly due to human interference, more so the burning of fossil fuels. The result is a worrying rise in the concentration of greenhouse gases in the air [4]. Emissions of carbon dioxide and other greenhouse gases have serious consequences for the planet, food production, disrupts natural habitats for animals, and even causes some of these extreme weather phenomena, such as tropical storms, wildfires, severe droughts, and warmer temperatures [5].

Understanding the primary sources of greenhouse gas emissions is essential for finding possibilities to reduce such emissions. The primary sources of greenhouse gas emissions are; plants that are used fossil fuels such as natural gas, coal, and crude oil to generate energy, agriculture, construction, transportation, and industries [6]. The burning of fossil fuels accounts for more than 80 percent of global greenhouse gas emissions, which produces carbon dioxide (CO<sub>2</sub>) [7]. Coal is the primary energy source used in the energy-intensive process of manufacturing steel. 7–9% of the direct carbon output from the usage of fossil fuels worldwide was caused

<sup>\*</sup> Corresponding author.

E-mail address: [Dalia.Amer@bue.edu.eg](mailto:Dalia.Amer@bue.edu.eg) (D. Amer Ali).

by the manufacturing of steel [7]. Emissions need be significantly reduced to meet the 2050 goal which is keeping global warming below 1.5 °C [8].

Carbon dioxide emissions are mitigated by several Research and Development (R&D) efforts aimed at reducing them [6,9]. A classification of its uses is; Production of chemicals (e.g., raw materials for polymers and carbonates). The second is the production of fuels (e.g., production of gasoline and diesel raw materials). The third is biological exploitation (e.g., a source of C for microalgae growth). The fourth is for conventional uses (such as solvents) [6,9].

Capturing carbon dioxide gas released by burning fossil fuels or organic materials requires four primary technologies as represented in Fig. 1: In pre-combustion capture, carbon is removed from the atmosphere before it is burned, post-combustion carbon capture removes carbon dioxide from flue gases through a variety of processes, including chemical absorption, physical adsorption, membrane separation, and cryogenic separation. While in oxy-combustion, carbon can be captured after combustion has taken place in an oxygen atmosphere (for example, using an oxygen gas turbine) [10–12]. When nitrogen is removed from the air prior to combustion, oxygen can be produced [10].

For CO<sub>2</sub> capture, a variety of methods are available, including membrane separation, cryogenics, adsorption, and absorption as represented in the following Fig. 2 [3,13]:

Adsorption process, when a gas or liquid flows past a solid absorbent, the absorbent's surface will take in some of those molecules. As the gas is pumped through the bed, the solid particles take up the elements it contains [14]. Given that the process generates heat, the adsorbents can be reused by increasing the temperature at which they are operated. These are the benefits of this process: It has fewer energy requirements, reduced operating costs, and a 90 % reduction in CO<sub>2</sub> emissions. On the other hand, the process configuration is difficult and the need of enormous amounts of energy to operate the process [6].

When the concentration of CO<sub>2</sub> in a stream is high, often greater than 50 %, cryogenic separation is often utilized to extract the gas [15]. This method's main benefits are that it could be applied at room temperature and pressure, and that no chemical adsorbent is necessary. It is challenging to employ this technology for CO<sub>2</sub> collecting due to the presence of other gases, such as sulphur oxides, nitrogen oxides, and water vapor, which significantly reduce cooling and lead to erosion, contamination, and clogging [12,13].

The membrane separation technique uses between 0.5 and 6 MJ kg<sup>-1</sup> of CO<sub>2</sub> removed, which is significantly less energy than is required by other available technologies. The membrane also acts as a semi-permeable barrier, controlling the diffusion of molecules between the two phases to create separation. The low CO<sub>2</sub> purity and removal efficiencies of this method render it inefficient, despite its low cost [12,16].

When the two phases in the mixture are gas and liquid, the absorption process can occur, which takes place on the combination between CO<sub>2</sub> and a chemical solvent. The benefits of this technology include absorbing CO<sub>2</sub> with an efficiency of around 90 % and the ability to handle a huge CO<sub>2</sub> stream [14,17].

The process of absorbing carbon dioxide using chemical solvents is known as chemical absorption [18]. When heated, solvents create an intermediate molecule with CO<sub>2</sub> that has a weak bond, which then releases the CO<sub>2</sub> that was previously trapped. The absorption process is often characterized by a high CO<sub>2</sub> selectivity and a significant capacity for absorption [13,17]. Additionally, it is the most extensively used and advanced form of CO<sub>2</sub> capture technology at the current time. The high expense and the extensive energy need for solvents regeneration are two of the primary challenges to the broad application of this process in coal-fired power plants and other large and medium-sized industrial emission sources. The low stability and aggressive corrosion are additional challenges, as are the high toxicity and high absorbent loss that result from these factors [13].

To overcome the limitations that stand in the way of CO<sub>2</sub> collection through solution absorption, extensive research on a global

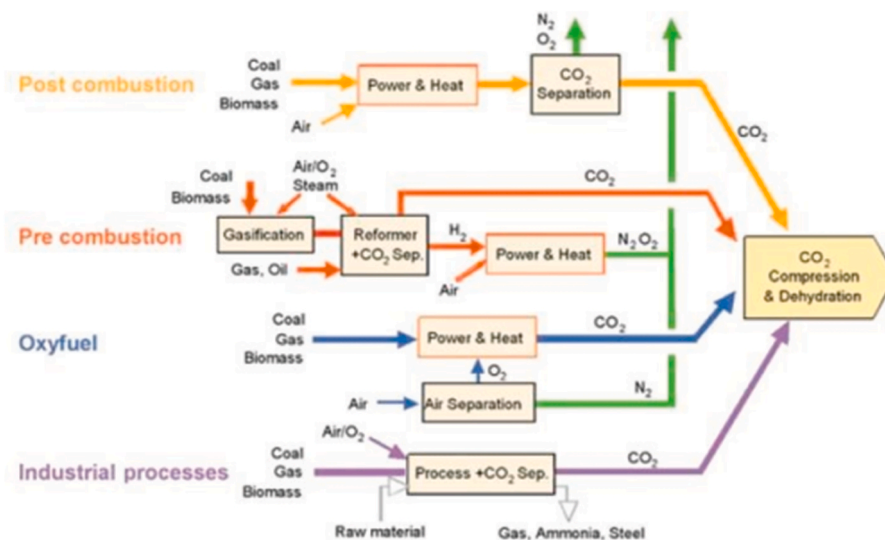


Fig. 1. CO<sub>2</sub> capture technologies.

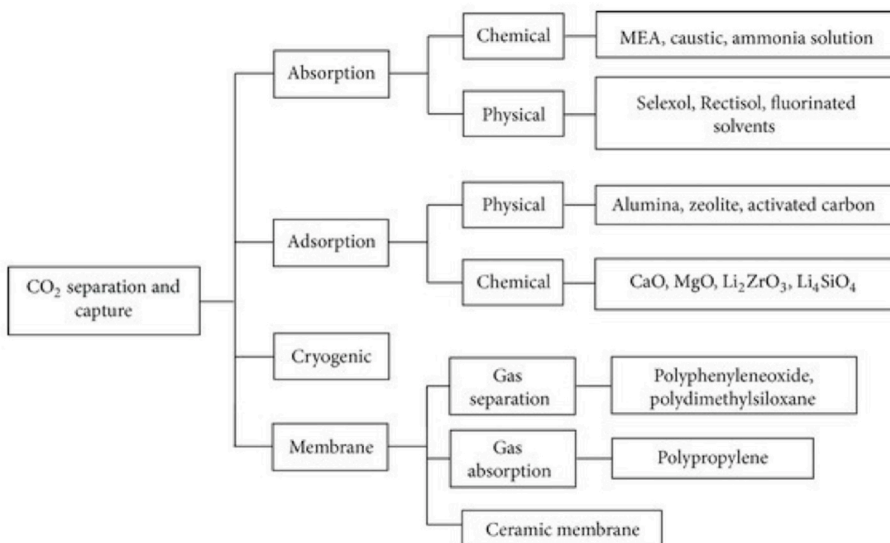


Fig. 2. CO<sub>2</sub> separation and capture methods.

scale has been carried out. CO<sub>2</sub> gas can be removed from natural gas through a chemical absorption process called natural gas sweetening using amines such as monoethanolamine (MEA) and diethanolamine (DEA) [15,18,19]. This process has some issues, such as a low CO<sub>2</sub> loading capacity, a high rate of equipment corrosion and amine degradation which cause a high absorbent replacement rate, high energy use when the absorbent is being regenerated at elevated temperatures and large equipment size [13,19].

The majority of CO<sub>2</sub> absorption studies in packed columns do not evaluate the interactive effects of operating variables in optimizing a single parameter [20,21]. Each independent process variable has a measurable effect on each other parameter in the CO<sub>2</sub> actual absorption process [20]. Therefore, independent variables must be identified in terms of their interactions. According to the Response Surface Methodology (RSM) a process variable's relative significance on the measured response can be determined economically [20]. Additionally, the use of a central composite response surface design (CCD) in combination with RSM provides a method of determining the behavior of process variables and predicting the optimum set of variables to use [20,21]. With reasonable numbers of experiments, this pathway reduces the time and cost of experiments [20].

In this research, instead of utilizing a chemical solvent like in the process of sweetening natural gas, a green absorbent was utilized in the form of sodium silicate extracted from sugarcane bagasse to transform carbon dioxide gas into silica and sodium carbonate using a designed apparatus.

## 2. Materials and methods

### 2.1. Chemicals

Sugarcane bagasse was collected from a farm at Al-Sharkeya governorate, Egypt. CO<sub>2</sub> gas cylinder was obtained from a food

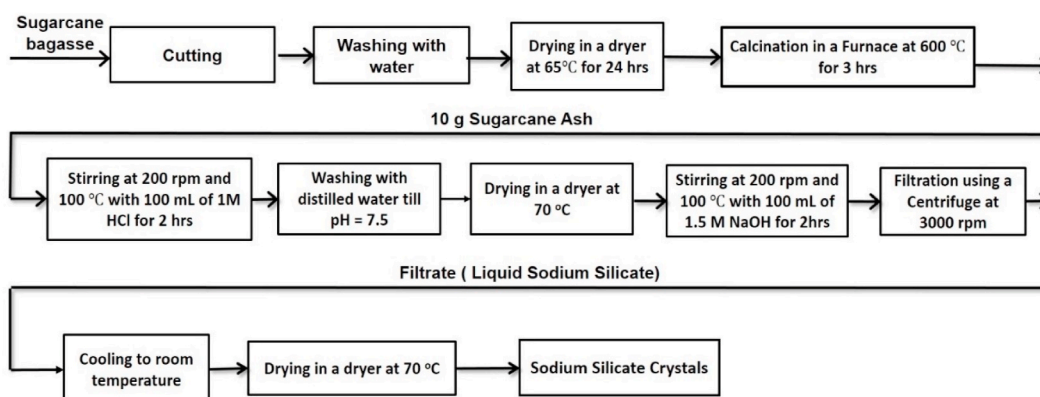


Fig. 3. Extraction scheme of sodium silicate from sugarcane bagasse.

packaging factory at 10th Ramadan city, Al-Sharkeya, Egypt. All chemicals used in this study were analytical grade reagents including sodium hydroxide (NaOH), Hydrochloric acid (HCl, 36 % v/v), silver nitrate solution (AgNO<sub>3</sub>) and Ammonium Chloride (NH<sub>4</sub>Cl, 99.5 %). These reagents were purchased from Sigma-Aldrich Company. Deionized water was used for preparation of all solutions.

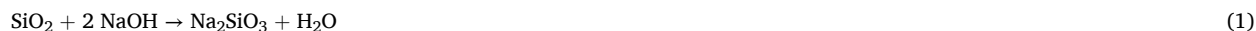
## 2.2. Equipment

The morphology of the extracted sodium silicate (Na<sub>2</sub>SiO<sub>3</sub>), the products silica (SiO<sub>2</sub>) and sodium carbonate (Na<sub>2</sub>CO<sub>3</sub>) were conducted by scanning electron microscope (SEM, Quattro s – Thermo Scientific, Netherland). The surface functional groups of the products SiO<sub>2</sub> and Na<sub>2</sub>CO<sub>3</sub> due to the CO<sub>2</sub> capture process were recorded using Fourier-transform infrared (FTIR) spectra (Vertex 70 RAM II, Germany). Filtration of SiO<sub>2</sub> was performed using vacuum filtration apparatus (RS-1, Shenzhen Educational Equipment, China). Vacuum dryer (Thermo-Fisher Scientific Company, USA) was used for drying the final product. The weight percentages of SiO<sub>2</sub> and Na<sub>2</sub>CO<sub>3</sub> were determined through gravimetric method [22].

## 2.3. Extraction of sodium silicate (Na<sub>2</sub>SiO<sub>3</sub>) from sugarcane bagasse

Fig. 3 represented the sodium silicate extraction process from sugarcane bagasse. Sugarcane bagasse was cut into smaller pieces, washed with water, dried at 65 °C for 24 h, and then calcined at 600 °C for 3 h. Using a two-neck bottle with a condenser, the extraction process was completed by mixing 10 g of sugarcane bagasse ash with 100 mL of 1 M HCl at 200 rpm with heating at 100 °C for 2 h, then washing in distilled water until reaching a neutral pH and drying in a dryer at 70 °C for 2 h. The previous step's product stirred with 100 mL NaOH (1.5 Molar) solution for 2 h at 100 °C. Sodium silicate crystals were then obtained by filtration in a centrifuge at 3000 rpm for 10 min, cooling to room temperature, drying at 70 °C in a dryer and storing in a desiccator.

In the previous steps the sugarcane ash which contained SiO<sub>2</sub> (52.67 %) and traces of other mineral salts as represented in Table 1 was acid treated using HCl to increase the weight percentage of SiO<sub>2</sub> and to decrease the other mineral oxides. After the acid treating of the sugarcane ash, an alkaline treatment occurred using 1 M NaOH for the SiO<sub>2</sub> to obtain sodium silicate (Na<sub>2</sub>SiO<sub>3</sub>) and water (H<sub>2</sub>O) as represented in the following reaction Eq. (1) [23]:



## 2.4. Apparatus

Continuous chemical absorption experiment of CO<sub>2</sub> gas using a green sodium silicate extracted from sugarcane bagasse was performed using a designed apparatus. Fig. 4 represented the apparatus setup used in the transformation of CO<sub>2</sub> gas into valuable product silica.

A packed bed column (B) of approximately 0.0035 m<sup>3</sup> volume is the main component of the apparatus. Inside the packed bed column (B), there is a support (O) with openings each with diameter of 1 mm and glass marbles (G) at certain height that act as the packing material. Injection of the aqueous sodium silicate solution into the bottom of the packed bed column is accomplished by a pump (P). This pump delivers a certain flow rate of aqueous sodium silicate solution from the feed tank (F) which has a volume of 0.0035 m<sup>3</sup> to the packed bed column (B). At the bottom of the packed bed column (B), the gas inlet pipe receives carbon dioxide gas that comes from the CO<sub>2</sub> gas cylinder (C). The carbon dioxide gas flow into the packed bed column (B) is controlled by valve (V1). A gas flowmeter (L) is used to measure the CO<sub>2</sub> gas flow rate enters the packed bed column. The sodium silicate solution flow into the packed bed column (B) is controlled by valve (V2). A product tank (T) with 0.0016 m<sup>3</sup> volume is used to collect the final gel product. A pH meter is used to measure the pH inside the packed bed column (B) throughout the reaction periods. A pressure gauge (P2) and a pressure gauge (P1) are used to measure the pressure difference across CO<sub>2</sub> gas cylinder (C) and the sodium silicate solution's pump (P).

Table 2 represented the main dimensions and specifications of the designed apparatus that was used in lab to perform the continuous chemical absorption process for CO<sub>2</sub> gas into silica using a green sodium silicate absorbent solution extracted from sugarcane bagasse.

## 2.5. Operating conditions selection

The choice of the studied parameter ranges in this research study, experiments was performed to determine conditions of Flooding as well as the allowable range of CO<sub>2</sub> gas flow rate and the allowable range of sodium silicate solution flow rate to be suitable with designed packed column. The packing sizes were chosen randomly to study their effect on the CO<sub>2</sub> gas absorption process using sodium

**Table 1**  
X-Ray Diffraction Analysis (XRF) of the sugarcane bagasse ash.

Material	SiO <sub>2</sub>	Al <sub>2</sub> O <sub>3</sub>	Fe <sub>2</sub> O <sub>3</sub>	CaO	MgO	SO <sub>3</sub>	Na <sub>2</sub> O	K <sub>2</sub> O	L.O.I	Total
%wt	52.67	10.45	9.59	8.79	4.16	0.02	3.82	0.64	6.24	96.38

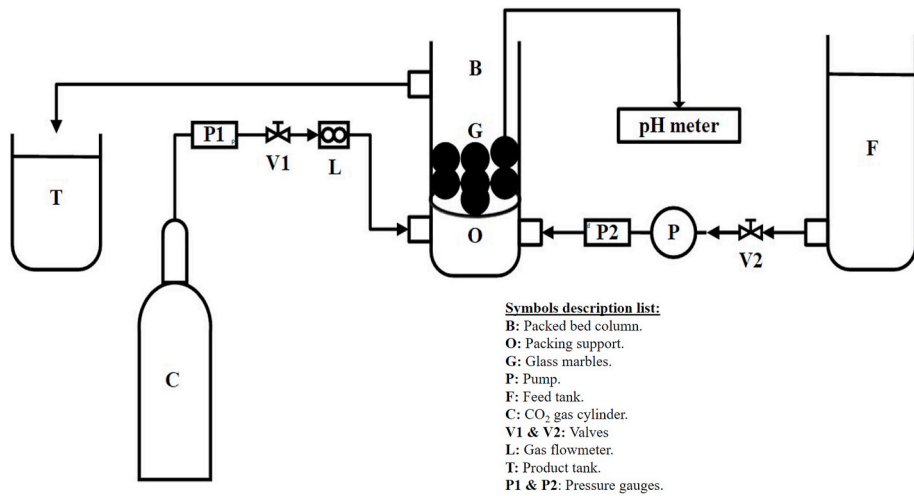


Fig. 4. The apparatus setup.

**Table 2**  
 Dimensions and specifications of the designed apparatus.

Unit	Dimensions/Specifications
Packed column	Height = 45 cm Diameter = 10 cm
Packing material (Marbles)	Large = 24.4 mm Medium = 20.175 mm Small = 15.95
Feed tank	Height = 45 cm Diameter = 10 cm
Product tank	Height = 20 cm Diameter = 10 cm
Pump	Rated Voltage = 220 V Speed Pange = 4200 rpm/min Rated Current = 12 A Rated Torque = 260 W
CO <sub>2</sub> feed gas cylinder	Volume = 40 L
CO <sub>2</sub> gas flowmeter	Maximum measured flow rate = 1.5 m <sup>3</sup> /h

silicate solution. Flooding phenomenon decreases significantly the efficiency of the absorption packed column, and it takes place at high gas and liquid flow rates.

The experiment procedure was performed in the designed apparatus at pressure 1 atm and 25 °C with a 0.045 m diameter column

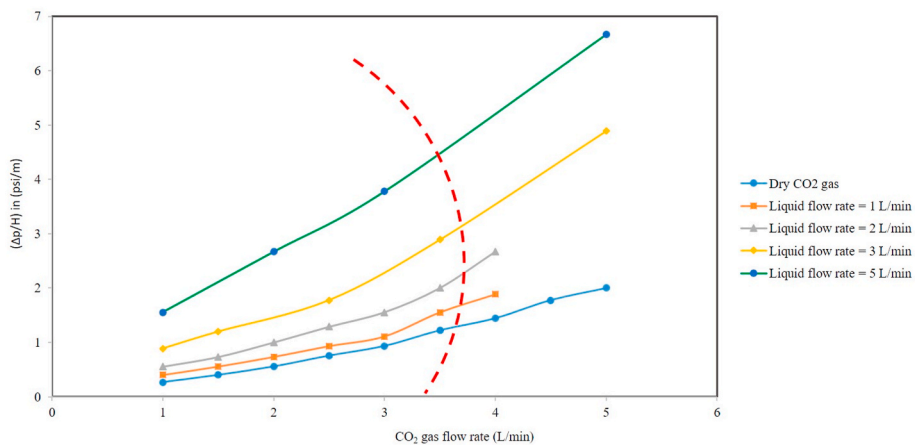


Fig. 5. Plot of  $(\Delta p/H)$  versus CO<sub>2</sub> gas flow rate for different sodium silicate solution flow rates.

randomly packed with 24.4 mm glass marbles to a height of 0.045 m as follows;

1. Operate the designed packed bed column with different dry flow rates of CO<sub>2</sub> gas in a range from 1 to 5 L/min only without flow of sodium silicate solution.
2. Measure the pressure drop across the designed packed bed column then plot a relation between ( $Q_{CO_2\text{gas}}$ ) in (L/min) on x-axis versus pressure drop ( $\Delta p/H$ ) in (psi/m) on y-axis, where H is the height of the packed column (m).
3. Operate the designed packed bed column with sodium silicate solution flow rate ranged from 1 to 5 L/min at each liquid solution flow rate, operate the system at different flow rates of CO<sub>2</sub> gas ranged from (1–5 L/min).
4. Measure the pressure drop across the designed packed bed column in each time then plot a relation between ( $Q_{CO_2\text{gas}}$ ) in (L/min) on (x-axis) versus pressure drop ( $\Delta p/H$ ) in (psi/m) on (y-axis).

Based on the plot represented in Fig. 5, it was preferred to operate the packed column at CO<sub>2</sub> gas and sodium silicate solution flow rates below the Flooding limit. Therefore, the safe range of CO<sub>2</sub> gas flow rate was 1–3.2 L/min while the safe range of sodium silicate solution was 1–3 L/min.

## 2.6. Material selection

The material of construction of the pump's internal body was made from stainless steel. The material of all pipes in this prototype were made from carbon steel. Acrylic was used as the material of construction for the feed tank, the packed bed column and the discharge or the product tank. All the selected materials were considered due to their corrosion resistance to sodium silicate solutions at high concentrations.

## 2.7. Testing procedure

This section described the testing procedure for the real designed prototype to evaluate its performance and to make sure that it operated successfully without failure occurrence in the pump and without any damage in the packed bed column and in the feed and product tanks.

At room temperature, operate the system with different CO<sub>2</sub> gas flowrates (1.035, 1.65 and 2.3 L/min) which were adjusted using the control valves and measured using a gas flowmeter followed by pouring of different concentrations of sodium silicate solution (5, 7.5 and 10 %wt) inside the feed tank then operate the pump to deliver the sodium silicate solution to the packed bed column where a chemical reaction between sodium silicate solution and CO<sub>2</sub> gas took place.

There were some specific considerations made to ensure accurate and reliable measurements included; controlling of the CO<sub>2</sub> gas flowrates from the gas column through adjustment of the gas pressure using a gauge pressure valve fixed on the top of the CO<sub>2</sub> column.

pH of the reaction medium inside the packed bed column has been measured throughout the reaction period as its value affected the production weight percentages of SiO<sub>2</sub> and Na<sub>2</sub>CO<sub>3</sub>.

After testing according to the above mentioned steps, it was observed that the designed prototype operated successfully without any damage in its parts. Also, it was observed that there was no leakage of solution from tanks, pump and pipes. In addition, SiO<sub>2</sub> was successfully produced as a main product from this prototype.

## 2.8. Safety considerations

Many safety precautions have been considered during the experimental setup and operation of the prototype to ensure the compliance with laboratory safety guidelines.

These safety precautions included; check on the gauge pressure valve fixed on the top of the CO<sub>2</sub> gas column to ensure that there was no gas leakage from it and to avoid extremely high gas pressure that might damage the parts of the apparatus during operation.

Check that there was no solution leakage from feed tank, product tank, the packed bed column, pipes and the pump.

Different high concentrations of sodium silicate solution were required to be prepared therefore, wearing gloves, lab coat and eye glass were mandatory due to its high corrosion nature.

## 2.9. Conversion process of CO<sub>2</sub> gas into SiO<sub>2</sub> and Na<sub>2</sub>CO<sub>3</sub>

This continuous chemical absorption process has been performed by changing three experimental factors including; the CO<sub>2</sub> gas flow rate, the packing size, and the initial concentration of sodium silicate (Na<sub>2</sub>SiO<sub>3</sub>) solution followed by recording the experimental results including; %wt of SiO<sub>2</sub>, %wt of Na<sub>2</sub>CO<sub>3</sub> and the reaction time.

To convert CO<sub>2</sub> gas into silica different concentrations of sodium metasilicate by weight percent was prepared (5, 7.5 and 10 %wt) using deionized water. A certain concentration of sodium silicate solution was poured into the feed tank then fed to the packed bed column through a pump. A certain flow rate of CO<sub>2</sub> gas from a CO<sub>2</sub> gas cylinder was fed to the packed bed column at room temperature. In the packed bed column, after the reaction between CO<sub>2</sub> gas and sodium silicate solution was completed, the product was collected and aged at room temperature for 24 h before being filtered using a vacuum filtration pump. Precipitate was then washed with deionized water, then dried at 45 °C in a vacuum dryer.

The possible mechanism that occurred when CO<sub>2</sub> gas encountered sodium silicate solution could be illustrated as shown in Fig. 6. At

the beginning of the absorption process,  $\text{CO}_2$  gas encountered with water molecules producing protons ( $\text{H}^+$ ) and carbonate ions ( $\text{CO}_3^-$ ). Due to decreasing in the pH during the absorption process, sodium ions ( $\text{Na}^+$ ) were replaced with protons ( $\text{H}^+$ ) forming salicylic acid ( $\text{H}_2\text{SiO}_3$ ) as well as sodium ions ( $\text{Na}^+$ ) combined with carbonate ions ( $\text{CO}_3^-$ ) forming sodium carbonate ( $\text{Na}_2\text{CO}_3$ ). It was observed during the experiment that at pH range from 5 to 6, a gel product was formed due to the oxidation-reduction (redox) reaction occurred between hydroxyl group ( $\text{OH}^-$ ) and salicylic acid, this observation was in agreement with literature [24]. Upon forming siloxane bonds ( $-\text{Si}-\text{O}-\text{Si}-$ ) between particles, a negative radius of curvature of the surface allows further deposit of silica at the contact point, resulting in particles of silica ( $\text{SiO}_2$ ).

### 2.10. Experimental design

Statistical Design of Experiments (DOE) is a powerful method for designing experiments that provide objective and reliable results. Two main uses of experimental setup were assessed to determine the variables that influence the experiment and its optimal conditions [25]. The regression and graphical analyses of the data were conducted with the aid of the Statistical Modelling Tool (SMT) from Stat-Ease Inc. (USA). The central Composite Design (CCD) design was highly adaptable and efficient, as it was able to provide extensive data on experimental variables and errors with the minimal experimental run-through time [26]. Additionally, additional axial and center points were included in the CCD design to improve simulation of response surface [26]. Consequently, multiple experiments in this research were conducted in accordance with the CCD design. To achieve the optimal levels of carbon dioxide gas flow rate, packing size and concentration sodium silicate solution, SMT was employed to analyse the response patterns and identify the most optimal combination of variables to generate optimal conditions. The number of experiments designed by CCD calculated by Eq. (2) [27]:

$$N = k^2 + 2k + n \quad (2)$$

where N is the total number of experiments, k is the number of factors studied, and n is the number of replicates.

The value of alpha in CCD is a critical factor to consider, as it can indicate the position of the axial points within the experimental domain. The design of a CCD is determined by the alpha value, which can be defined as spherical or orthogonal. Additionally, the design can be rotatable, or face centered, and is typically in between the two. Therefore, the design is calculated as in Eq. (3) [27]:

$$\alpha = (2^k)^{0.25} \quad (3)$$

Alpha = 1 is a good number because it makes sure the axial point is in the right spot in the factorial part of the design. This type of design, known as face centered design, has three levels of factors to include in the design matrix [27]. It is possible to describe the

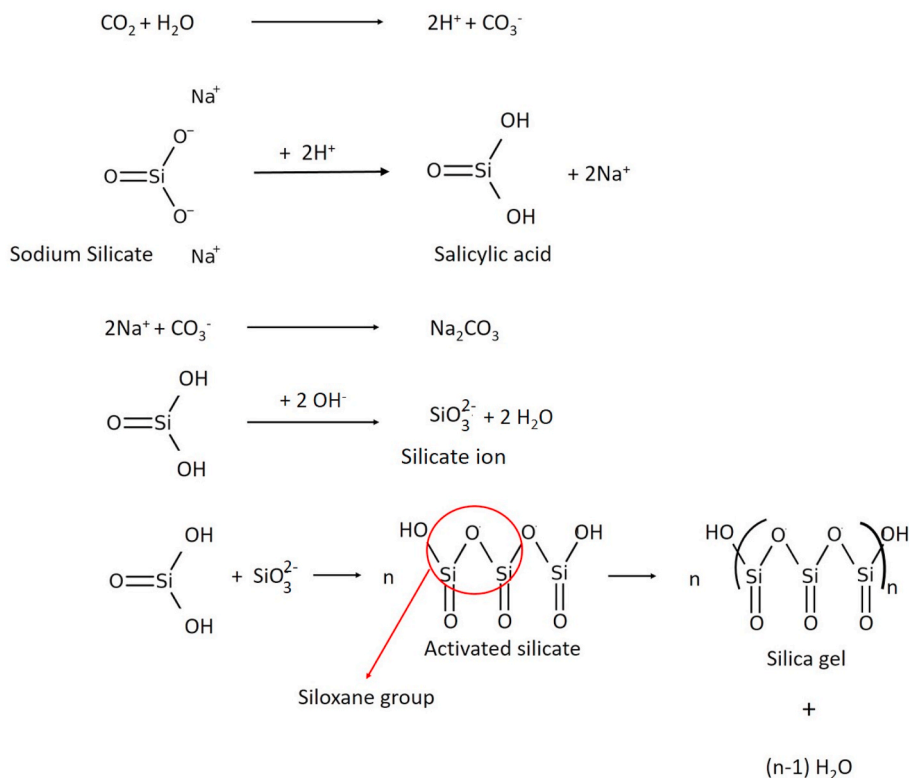


Fig. 6. Silica gel production mechanism in  $\text{CO}_2$  gas absorption process using sodium silicate solution.

behavior of a system mathematically by describing the relationship between inputs and outputs. Quadratic model, or second-order polynomial model, can be used to describe the system’s behavior. This model takes the form of Eq. (4) [27,28]:

$$Y = \beta_0 + \sum_{i=1}^k \beta_i x_i + \sum_{i=1}^k \beta_{ii} x_i^2 + \sum_{i=1}^k \sum_{j=1}^k \beta_{ij} x_i x_j + \epsilon \tag{4}$$

Here, Y represents the responses, k is the total number independent factors,  $\beta_0$  is an intercept, i, ii, and ij with  $\beta$  represent the coefficient values for linear, quadratic, and interaction effects, respectively, and xi and xj in the above equation show the coded levels for independent variables. For this research, Eq. (4) is written as Eq. (5) [27,28]:

$$Y_i = \beta_0 + \beta_1 x_1 + \beta_2 x_2 + \beta_3 x_3 + \beta_{11} x_{21} + \beta_{22} x_{22} + \beta_{33} x_{23} + \beta_{12} x_1 x_2 + \beta_{13} x_1 x_3 + \beta_{23} x_2 x_3 \tag{5}$$

Table 3 represented the experimental design matrix generated by (CCD) for the weight percent of SiO<sub>2</sub>, weight percent of Na<sub>2</sub>CO<sub>3</sub> and the reaction time responses. The Analysis of Variance (ANOVA) and multiple regression analyses in the Central Composite Design (CCD) with quadratic model Eq. (5) were performed based on the data represented in Table 3.

### 3. Results and discussion

#### 3.1. Surface characterization

Surface characterization including Scanning Electron Microscopy (SEM) analysis was performed after extraction of sodium silicate from sugarcane bagasse and after the continuous chemical absorption process of CO<sub>2</sub> gas in a packed bed column to give a description of the produced silica (SiO<sub>2</sub>) and sodium carbonate (Na<sub>2</sub>CO<sub>3</sub>).

##### 3.1.1. Scanning Electron Microscopy (SEM) of sodium silicate (Na<sub>2</sub>SiO<sub>3</sub>)

Fig. 7 represented the SEM of the extracted Na<sub>2</sub>SiO<sub>3</sub> from sugarcane bagasse. It illustrated the heterogeneous and porous surface with spherical particles that had the same diameter.

##### 3.1.2. Scanning Electron Microscopy (SEM) of the produced silica (SiO<sub>2</sub>) and sodium carbonate (Na<sub>2</sub>CO<sub>3</sub>)

Fig. 8 represented the surface micro-structure of the produced silica (SiO<sub>2</sub>) and sodium carbonate (Na<sub>2</sub>CO<sub>3</sub>). The silica particles appeared as flakes or thick layers in the form of irregular lumps and particles of sodium carbonate appear in spherical shapes with some agglomeration. The Fig. 8a was at 5 μm which represented the flakes of the silica particles in an obvious way while Fig. 8b was at 4 μm represented the spherical particles of sodium carbonate in a more obvious way.

##### 3.1.3. Fourier transform infrared (FTIR)

Fig. 9 represented the FTIR of the products due to the chemical absorption process of CO<sub>2</sub> gas in a packed bed column using sodium silicate solution as this analysis was performed at wavelength ranges from 400 to 4000 cm<sup>-1</sup>. The IR band at wavelength of 1669.49

**Table 3**

Experimental design matrix generated by Central Composite Design (CCD) for the weight percent (%wt) of SiO<sub>2</sub>, the weight percent (%wt) of Na<sub>2</sub>CO<sub>3</sub> and the reaction time.

Run	A: CO <sub>2</sub> gas flow rate L/min	B: Packing size mm	C: Initial concentration of sodium silicate %wt	Y1: Experimental %wt of SiO <sub>2</sub> %wt	Y2: Experimental %wt of Na <sub>2</sub> CO <sub>3</sub> %wt	Y3: Experimental reaction time min
1	1.6485	20.175	7.5	20.89	14.03	13
2	1.6485	20.175	5	22.22	15.28	12
3	1.6485	20.175	7.5	20.89	14.03	13
4	1.037	15.95	10	7.86	27.4	9
5	1.6485	20.175	7.5	20.89	14.03	13
6	2.26	20.175	7.5	4.42	30.85	24
7	1.6485	15.95	7.5	17.84	18.98	18
8	1.6485	24.4	7.5	23.77	12.72	11
9	1.037	15.95	5	6.19	32.53	11
10	2.26	15.95	10	2.63	32.047	26
11	1.037	24.4	10	15.18	23.09	5
12	1.6485	20.175	7.5	20.89	14.03	13
13	2.26	24.4	5	3.24	27.56	20
14	1.6485	20.175	10	25.82	9.31	8
15	1.037	24.4	5	12.36	24.77	7
16	2.26	15.95	5	1.52	35.77	28
17	1.6485	20.175	7.5	20.89	14.03	13
18	2.26	24.4	10	5.1	25.14	19
19	1.6485	20.175	7.5	20.89	14.03	13
20	1.037	20.175	7.5	9.89	25.53	10

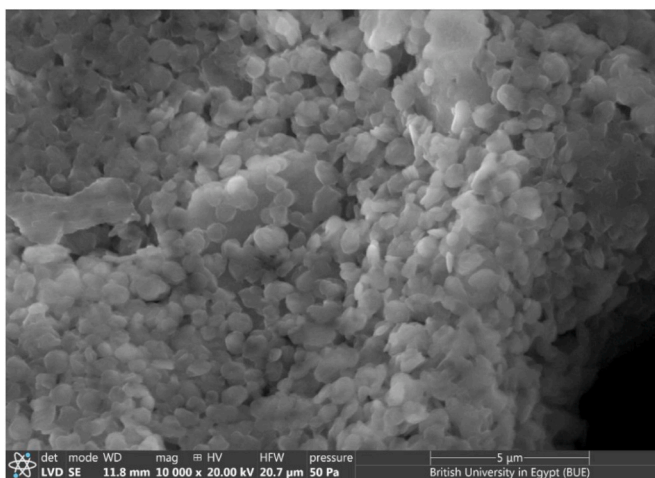


Fig. 7. SEM of sodium silicate extracted from sugarcane bagasse.

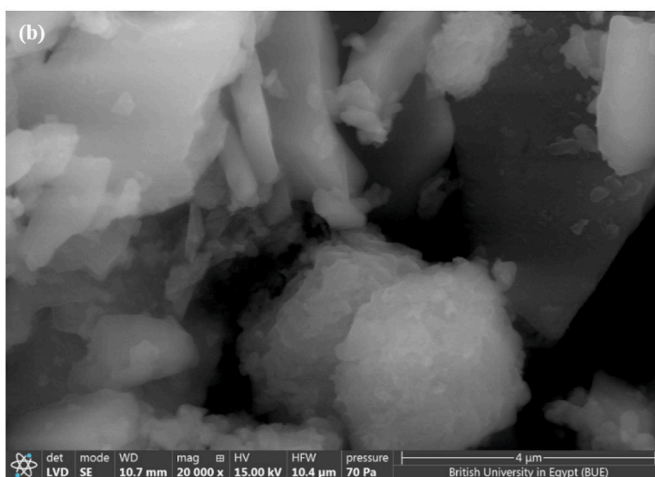
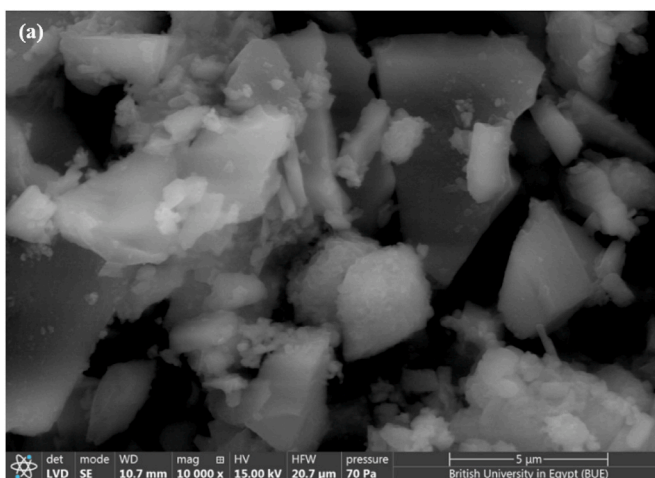


Fig. 8. SEM of silica ( $\text{SiO}_2$ ) and sodium carbonate ( $\text{Na}_2\text{CO}_3$ ) products (a) at 5  $\mu\text{m}$  and (b) at 4  $\mu\text{m}$ .

$\text{cm}^{-1}$  revealed C–O (Carbonyl group) [29]. While the sharp peaks at  $849.81 \text{ cm}^{-1}$ ,  $865.59 \text{ cm}^{-1}$ ,  $1446.26 \text{ cm}^{-1}$  and  $1408.28 \text{ cm}^{-1}$  revealed to the  $\text{CO}_3^{2-}$  (Carbonate group) which confirmed the presence of  $\text{Na}_2\text{CO}_3$  as a side product or contaminant with  $\text{SiO}_2$  [30]. The sharp peak at  $849.81 \text{ cm}^{-1}$  revealed to Si–C [31]. The sharp peak at  $460.44 \text{ cm}^{-1}$  revealed to the unsymmetrical Si–O–Si stretching vibration bonding [31,32]. The sharp peak at  $1027.38 \text{ cm}^{-1}$  revealed the  $\text{SiO}_4^{2-}$  group [33,34]. Therefore, Fig. 9 confirmed the production of  $\text{SiO}_2$  and  $\text{Na}_2\text{CO}_3$  from the reaction between  $\text{CO}_2$  gas and  $\text{Na}_2\text{SiO}_3$  in a packed bed column under controlled conditions of  $\text{CO}_2$  gas flow rate, packing size and initial concentration of sodium silicate solution. This FTIR analysis was agreed with a study reported by Ref. [30].

### 3.2. Regression model equations development

The best fitted model with the experimental results was the quadratic model. This best fitted model has been determined using the Design Expert software program, USA (Version 13). The model that was chosen to determine the best fitted model for this chemical absorption system was the Response Surface Methodology - Central Composite Design (RSM-CCD). The effects of three experimental factors were studied including, the  $\text{CO}_2$  gas flow rate (L/min), the packing size (mm) and the initial concentration of sodium silicate ( $\text{Na}_2\text{SiO}_3$ ) (%wt). Three responses were detected experimentally including; %wt of  $\text{SiO}_2$  product, %wt of  $\text{Na}_2\text{CO}_3$  product and the reaction time (min).

Table 3 illustrated that the maximum experimental value of the %wt of  $\text{SiO}_2$  was 25.82 % while its minimum value was 1.52 %. The maximum experimental value of the %wt of  $\text{Na}_2\text{CO}_3$  was 35.77 % while its minimum value is 9.31 %. The maximum value of the reaction time was 28 min while its minimum value was 5 min.

The quadratic model for %wt of  $\text{SiO}_2$  after removal of insignificant terms to increase the model's accuracy could be represented in the following Eq. (6):

$$Y_1 = +21.39 - 3.46 A + 2.36 B + 1.11 C - 1.16 AB - 14.99 A^2 - 1.34 B^2 + 1.88 C^2 \quad (6)$$

The quadratic model for %wt of  $\text{Na}_2\text{CO}_3$  after removal of insignificant terms to increase the model's accuracy could be represented in the following Eq. (7):

$$Y_2 = +13.99 - 1.80 A - 3.34 B - 1.89 C + 0.5941 BC + 14.26 A^2 + 1.92 B^2 - 1.64 C^2 \quad (7)$$

The quadratic model for reaction time after removal of insignificant terms to increase the model's accuracy could be represented in the following Eq. (8):

$$Y_3 = +12.98 + 7.5 A - 3.00 B - 1.10 C - 0.8750 AB + 4.05 A^2 + 1.55 B^2 - 2.95 C^2 \quad (8)$$

Where  $Y_1$ ,  $Y_2$  and  $Y_3$  are the %wt of  $\text{SiO}_2$ , %wt of  $\text{Na}_2\text{CO}_3$  and the reaction time, respectively. A, B and C are the  $\text{CO}_2$  gas flow rate (L/min), the packing size (mm) and the initial concentration of sodium silicate ( $\text{Na}_2\text{SiO}_3$ ) (%wt), respectively.

The positive and negative signs indicated that actual experimental factors had direct and inverse proportional with the %wt of  $\text{SiO}_2$ , %wt of  $\text{Na}_2\text{CO}_3$  and the reaction time.

#### 3.2.1. ANOVA for the quadratic model of the %wt of $\text{SiO}_2$

Predicted models were checked for adequacy using different methods [27]. As represented in Table 4, a value of 0.9933 was obtained for  $R^2$ , 0.9874 was obtained for  $R_{\text{adjusted}}^2$ , while a value of 0.9624 was obtained for  $R_{\text{predicted}}^2$ . If  $R^2$  was near unity, the model could accurately predict the actual data. As the p-value of the predicted model was less than 0.0001, it was Highly Significant (HS). Table 4 illustrated that all parameters with p-values less than 0.05 were considered Significant (S).

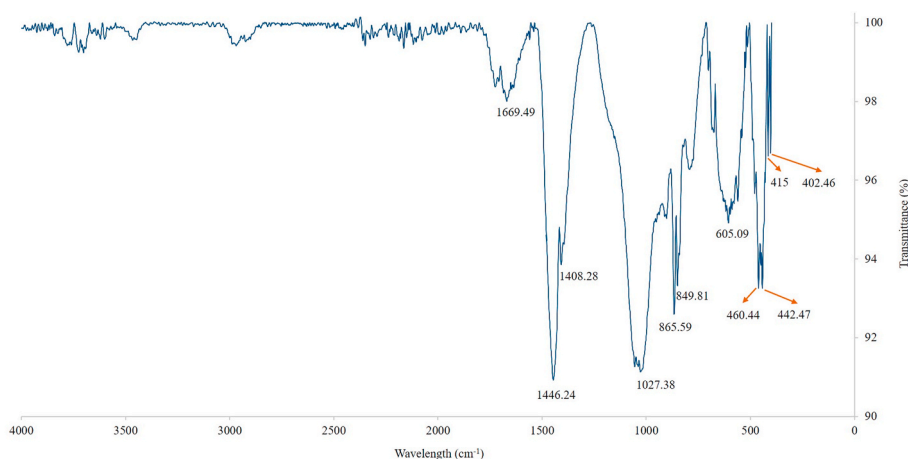


Fig. 9. FTIR of silica ( $\text{SiO}_2$ ) and sodium carbonate ( $\text{Na}_2\text{CO}_3$ ).

**Table 4**  
The Analysis of Variance (ANOVA) of the weight percent (%wt) of SiO<sub>2</sub>.

Source	Sum of Squares	df	Mean Square	F-value	p-value	
Model	1284.60	9	142.73	165.91	<0.0001	HS
A-CO <sub>2</sub> Gas flow rate	119.51	1	119.51	138.91	<0.0001	HS
B-Packing Size	55.74	1	55.74	64.79	<0.0001	HS
C-Initial Concentration of sodium silicate	12.23	1	12.23	14.22	0.0037	S
AB	10.81	1	10.81	12.57	0.0053	S
AC	0.2888	1	0.2888	0.3357	0.5751	NS
BC	0.4513	1	0.4513	0.5245	0.4855	NS
A <sup>2</sup>	617.59	1	617.59	717.87	<0.0001	HS
B <sup>2</sup>	4.91	1	4.91	5.70	0.0381	S
C <sup>2</sup>	9.71	1	9.71	11.29	0.0072	S
Residual	8.60	10	0.8603			
Lack of Fit	8.60	5	1.72			
Pure Error	0.0000	5	0.0000			
Core Total	1293.20	19				

The Model F-value of 165.91 implied the model was significant. In this case A, B, C, AB, A<sup>2</sup>, B<sup>2</sup>, C<sup>2</sup> were significant model terms. Values greater than 0.05 indicated the model terms were Non-Significant (NS).

3.2.1.1. *Effect of process variables and response surface contour plots in %wt of SiO<sub>2</sub> model.* Response surface curves are used to give a complete characterization of the system with several inputs and outputs.

a) Effect of CO<sub>2</sub> gas flow rate

Table 4 showed that the CO<sub>2</sub> gas flow rate had a high significant impact on the produced %wt of SiO<sub>2</sub>. As represented in the Fig. 10, when the CO<sub>2</sub> gas flow rate increased from 1.1 L/min to 1.648 L/min, the weight percentage of the produced SiO<sub>2</sub> increased from 10 % to 20 %. But more increase in the CO<sub>2</sub> gas flow rate from 1.648 L/min to 2.2 L/min resulted in a decrease in the produced %wt of SiO<sub>2</sub> from 20 % to 5 % at various levels of packing size and under fixed initial sodium silicate concentration of 7.5 wt%. Because, when the CO<sub>2</sub> gas flow rate increased till reaching 1.648 L/min, the pH of the reaction medium decreased till reaching pH = 6 which resulted in precipitation of SiO<sub>2</sub> particles. While with further increase in the CO<sub>2</sub> gas flow rate, the pH decreased to be lower than 6 promoting formation of silicic acid (H<sub>4</sub>SiO<sub>4</sub>) which was soluble in water. In addition, extremely low pH promoted precipitation of more Na<sub>2</sub>CO<sub>3</sub> rather than SiO<sub>2</sub> and this took place due to the formation of carbonic acid (H<sub>2</sub>CO<sub>3</sub>) which reacted with sodium ions exit in the solution.

b) Effect of the packing size

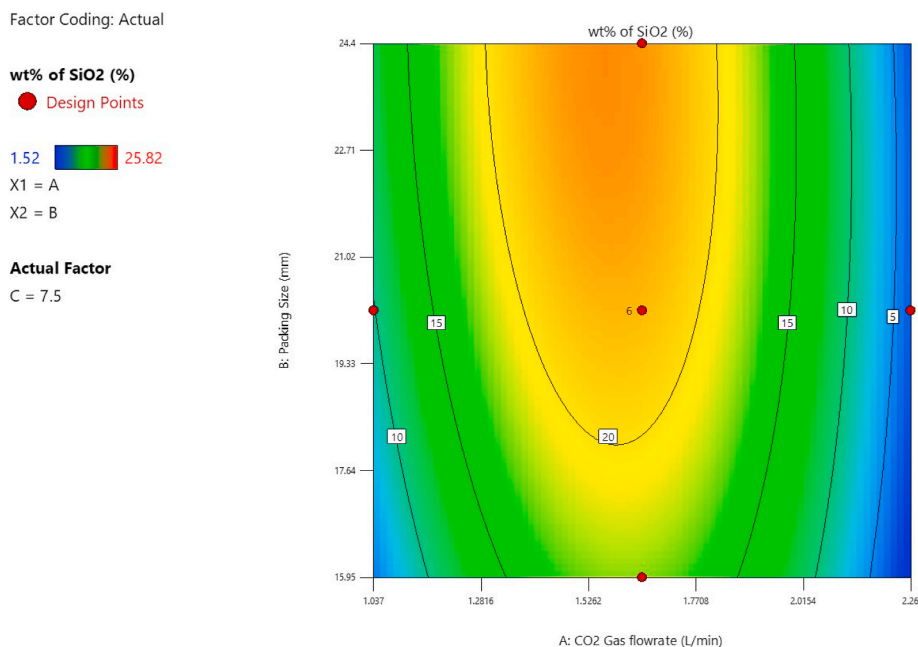


**Fig. 10.** Contour plot of the CO<sub>2</sub> gas flow rate and the packing size versus the %wt of SiO<sub>2</sub>.

Based on Table 4, the packing size affected the produced %wt of SiO<sub>2</sub>. According to the regression Eq. (6), the packing size and the produced %wt of SiO<sub>2</sub> were directly proportional. Fig. 11 illustrated that when the packing size increased from 15.95 mm to 24.4 mm, the %wt of SiO<sub>2</sub> was slightly increased from 18 % to 24 % at various levels of initial concentration of sodium silicate and under fixed CO<sub>2</sub> gas flow rate of 1.648 L/min. This occurred because, the glass marbles contained silica. Therefore, the CO<sub>2</sub> gas not only reacted with the sodium silicate solution to precipitate silica but also, it precipitated some of silica existed in the glass marbles packing.

### 3.2.2. ANOVA for the quadratic model of the %wt of Na<sub>2</sub>CO<sub>3</sub>

As represented in Table 5, a value of 0.9955 was obtained for R<sup>2</sup>, 0.9915 was obtained for R<sub>adjusted</sub><sup>2</sup>, while a value of 0.9583 was obtained for R<sub>predicted</sub><sup>2</sup>. If R<sup>2</sup> was near unity, the model could accurately predict the actual data. As the p-value of the predicted model was less than 0.0001, it was Highly Significant (HS). Table 5 showed that all parameters with a p-value higher than 0.05 are considered Non-Significant (NS).

The Model F-value of 248.3 implied the model was significant. P-values less than 0.0500 indicate model terms were Significant (S). In this case A, B, C, BC, A<sup>2</sup>, B<sup>2</sup>, C<sup>2</sup> were significant model terms.

#### 3.2.2.1. Effect of process variables and response surface contour plots in %wt of Na<sub>2</sub>CO<sub>3</sub> model.

##### a) Effect of CO<sub>2</sub> gas flow rate

Table 5 showed that the CO<sub>2</sub> gas flow rate had a high significant impact on the produced %wt of Na<sub>2</sub>CO<sub>3</sub>. As per represented in the Fig. 12, when the CO<sub>2</sub> gas flow rate increased from 1.037 L/min to 1.648 L/min, the weight percent of the produced Na<sub>2</sub>CO<sub>3</sub> decreased from 30 % to 15 %. More increase in the CO<sub>2</sub> gas flow rate from 1.648 L/min to 2.2 L/min resulted in increasing in the produced %wt of Na<sub>2</sub>CO<sub>3</sub> from 15 % to 30 % at various levels of packing sizes and under fixed initial sodium silicate concentration of 7.5 %wt. Because, when the CO<sub>2</sub> gas flow rate increased from 1.037 L/min to 1.648 L/min, the pH of the reaction medium decreased from 12 to 6 which promoted precipitation of SiO<sub>2</sub> and resisted the precipitation of Na<sub>2</sub>CO<sub>3</sub> particles. As the CO<sub>2</sub> gas flow rate increased beyond 1.648 L/min, the pH decreased to less than 6, which was more suitable for Na<sub>2</sub>CO<sub>3</sub> precipitation due to the formation of carbonic acid (H<sub>2</sub>CO<sub>3</sub>) that reacted with sodium ions existed in the solution.

##### b) Effect of the packing size

Based on Table 5, the packing size significantly affected the produced %wt of Na<sub>2</sub>CO<sub>3</sub>. According to the regression Eq. (7), the packing size and the produced %wt of Na<sub>2</sub>CO<sub>3</sub> were inversely proportional. Fig. 13 illustrated that when the packing size increased from 15.95 mm to 24.4 mm, the %wt of Na<sub>2</sub>CO<sub>3</sub> decreased from 18 % to 10 % at various levels of initial concentration of sodium silicate and under fixed CO<sub>2</sub> gas flow rate of 1.648 L/min. When the packing size increased, this resulted in increasing the precipitation of SiO<sub>2</sub> not Na<sub>2</sub>CO<sub>3</sub>. Due to the presence of sodium silicate solution and the silica contained in the glass marbles, the CO<sub>2</sub> gas reacted with sodium silicate solution to precipitate silica. Also, it enhanced the precipitation of silica that existed already in the glass marbles packing.

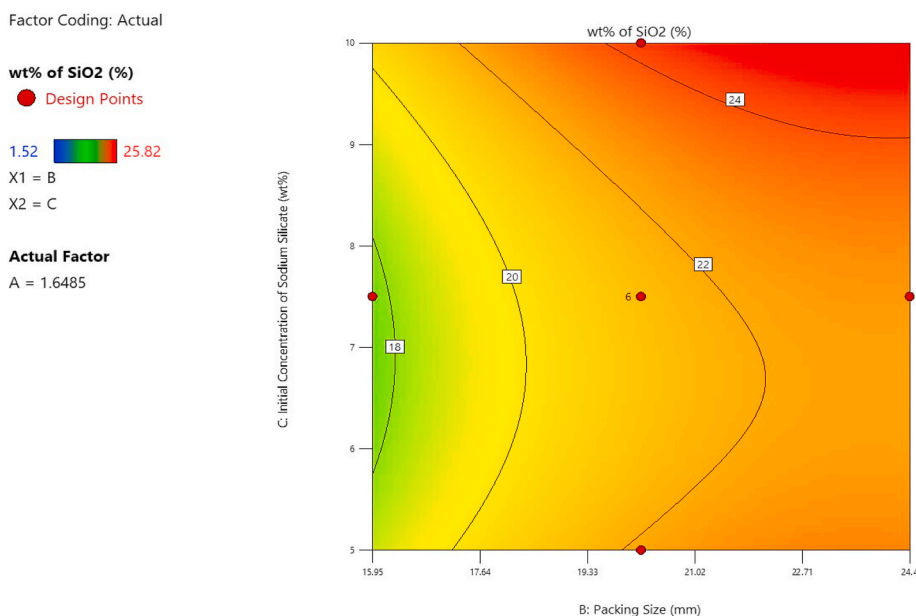
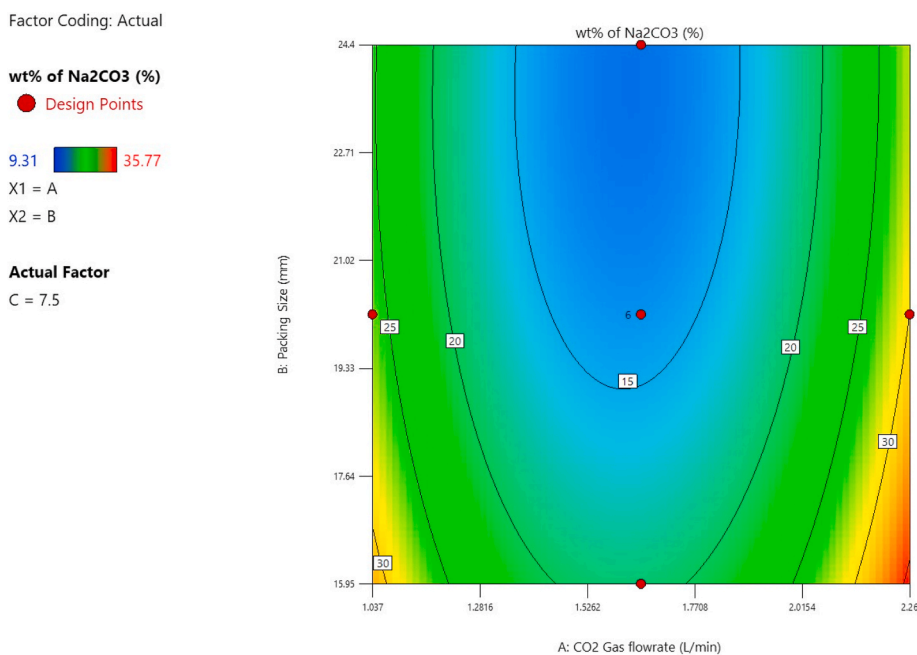


Fig. 11. Contour plot of the packing size and the initial concentration of sodium silicate versus the weight percent (%wt) of SiO<sub>2</sub>.

**Table 5**  
The Analysis of Variance (ANOVA) of the weight percent (%wt) of  $\text{Na}_2\text{CO}_3$ .

Source	Sum of Squares	df	Mean Square	F-value	p-value	
Model	1237.02	9	137.45	248.30	<0.0001	HS
A-CO <sub>2</sub> Gas flowrate	32.57	1	32.57	58.84	<0.0001	HS
B-Packing Size	111.87	1	111.87	202.09	<0.0001	HS
C-Initial Concentration of sodium silicate	35.81	1	35.81	64.69	<0.0001	HS
AB	1.16	1	1.16	2.10	0.1783	NS
AC	0.0556	1	0.0556	0.1005	0.7578	NS
BC	2.82	1	2.82	5.10	0.0475	S
A <sup>2</sup>	558.87	1	558.87	1009.61	<0.0001	HS
B <sup>2</sup>	10.09	1	10.09	18.23	0.0016	S
C <sup>2</sup>	7.39	1	7.39	13.35	0.0044	S
Residual	5.54	10	0.5536			
Lack of Fit	5.54	5	1.11			
Pure Error	0.0000	5	0.0000			
Core Total	1242.56	19				



**Fig. 12.** Contour plot of the CO<sub>2</sub> gas flow rate and the packing size versus the weight percent (%wt) of  $\text{Na}_2\text{CO}_3$ .

### c) Effect of the initial sodium silicate concentration

Based on Table 5, the initial sodium silicate concentration significantly affected the produced %wt of  $\text{Na}_2\text{CO}_3$ . According to the regression Eq. (7), the initial sodium silicate concentration and the produced %wt of  $\text{Na}_2\text{CO}_3$  were inversely proportional. Fig. 14 illustrated that when the initial sodium silicate concentration increased from 9 %wt to 10 %wt, the weight percent of  $\text{Na}_2\text{CO}_3$  decreased from 25 % to 20 % at CO<sub>2</sub> gas flow rate range of 1.037 L/min to 1.1 L/min and under fixed packing size of 20.175 mm. Because sodium silicate ( $\text{Na}_2\text{SiO}_3$ ) was a mixture of  $\text{SiO}_2$  and  $\text{Na}_2\text{O}$ , an increase in sodium silicate concentration at the CO<sub>2</sub> gas flow rate less than 1.648 L/min and at fixed packing size resulted in a greater weight percent of the produced  $\text{SiO}_2$  not  $\text{Na}_2\text{CO}_3$ .

#### 3.2.3. ANOVA for the quadratic model of the reaction time

As represented in Table 6, a value of 0.9955 was obtained for  $R^2$ , 0.9914 was obtained for  $R^2_{\text{adjusted}}$ , while a value of 0.9622 was obtained for  $R^2_{\text{predicted}}$ . If  $R^2$  was near unity, the model could accurately predict the actual data. As the p-value of the predicted model was less than 0.0001, it was highly significant. Table 6 showed that all parameters with a p-value less than 0.05 were considered Non-Significant (NS).

The Model F-value of 243.56 implied the model had significant. P-values less than 0.0500 indicate model terms were significant. In this case A, B, C, AB, A<sup>2</sup>, B<sup>2</sup>, C<sup>2</sup> were significant model terms. Values greater than 0.1000 indicated the model terms were not significant.

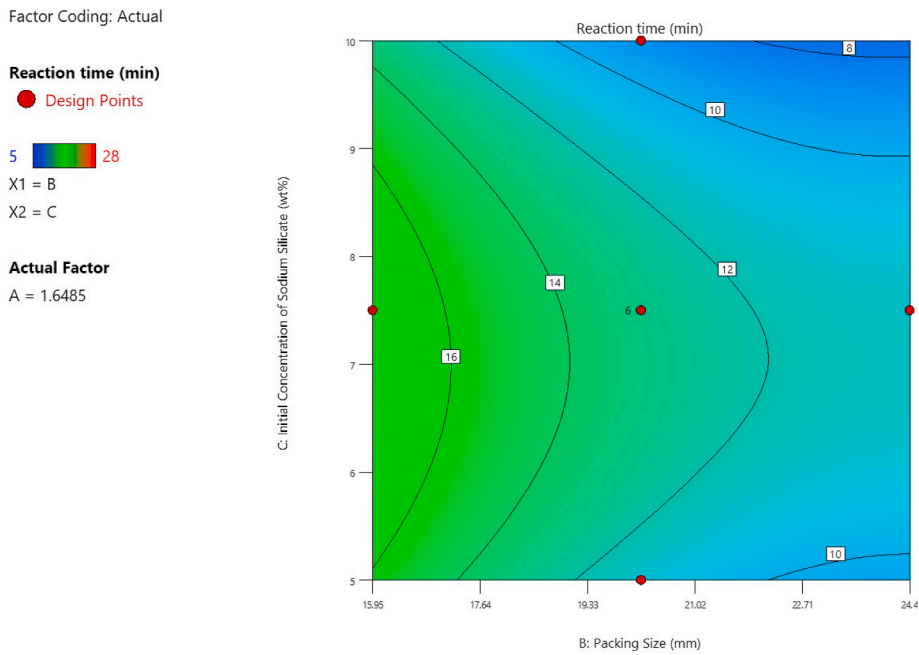


Fig. 13. Contour plot of the packing size and the initial concentration of sodium silicate versus the weight percent (%wt) of  $\text{Na}_2\text{CO}_3$ .

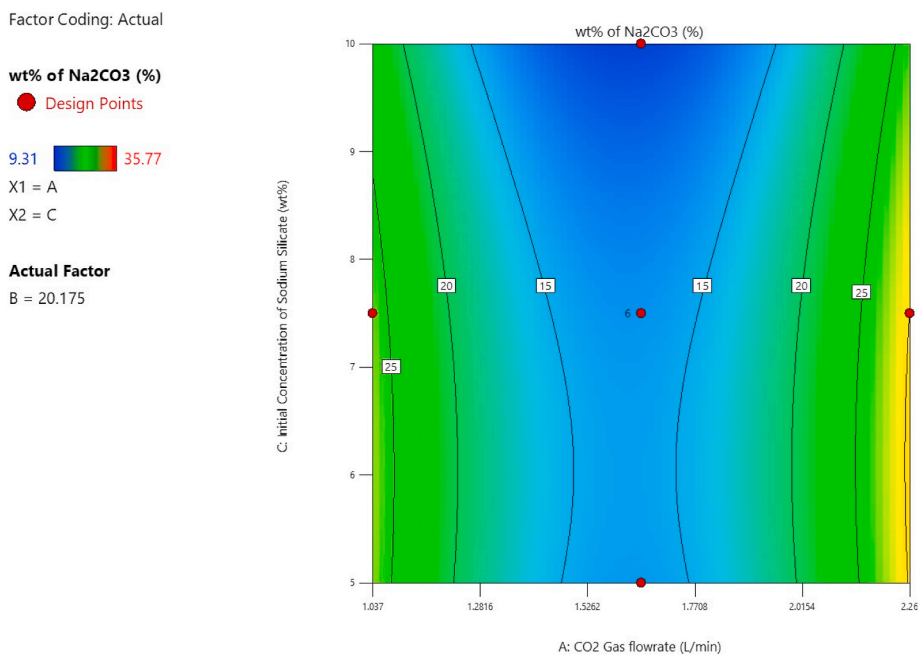


Fig. 14. Contour plot of the  $\text{CO}_2$  gas flow rate and the initial concentration of sodium silicate versus the weight percent (%wt) of  $\text{Na}_2\text{CO}_3$ .

3.2.3.1. Effect of process variables and response surface contour plots in the reaction time model.

a) Effect of  $\text{CO}_2$  gas flow rate

Table 6 showed that the  $\text{CO}_2$  gas flow rate had a high significant impact on the produced %wt of  $\text{SiO}_2$ . As per represented in the Fig. 15, when the  $\text{CO}_2$  gas flow rate increased from 1.52 L/min to 2.2 L/min, the reaction time increased from 15 % to 25 % at various levels of packing size and at fixed initial concentration of sodium silicate 7.5 %wt. Because increasing in the  $\text{CO}_2$  gas flow rate enhanced the precipitation of silica from sodium silicate solution at fixed other factors led to longer reaction time. This observation was

**Table 6**

The Analysis of Variance (ANOVA) of the reaction time.

Source	Sum of Squares	DF	Mean Square	F-value	p-value	
Model	746.79	9	82.98	243.56	<0.0001	HS
A-CO <sub>2</sub> Gas Flow rate	562.50	1	562.50	1651.10	<0.0001	HS
B-Packing Size	90.00	1	90.00	264.18	<0.0001	HS
C-Initial Concentration of sodium silicate	12.10	1	12.10	35.52	0.0001	HS
AB	6.13	1	6.13	17.98	0.0017	S
AC	0.1250	1	0.1250	0.3669	0.5582	NS
BC	0.1250	1	0.1250	0.3669	0.5582	NS
A <sup>2</sup>	45.01	1	45.01	132.10	<0.0001	HS
B <sup>2</sup>	6.57	1	6.57	19.28	0.0014	S
C <sup>2</sup>	24.01	1	24.01	70.46	<0.0001	HS
Residual	3.41	10	0.3407			
Lack of Fit	3.41	5	0.6814			
Pure Error	0.0000	5	0.0000			
Core Total	750.20	19				

agreed with a study reported by Ref. [30] where the effect of reaction time on silica yield was studied as the reaction time varied from 30 to 180 min with the Na<sub>2</sub>SiO<sub>3</sub> concentration of 0.5 mol/L and temperature at 70 °C while fixing other factors. The silica yield increases with increasing reaction time.

#### b) Effect of the packing size

Based on Table 6, the packing size significantly affected the reaction time. According to the regression Eq. (8), the packing size and the reaction time were inversely proportional. Fig. 16 illustrated that when the packing size increased from 15.95 mm to 19 mm, the reaction time decreased from 16 min to 12 min at various levels of initial concentration of sodium silicate and under fixed CO<sub>2</sub> gas flow rate of 1.648 L/min. When the packing size increased, this resulted in increasing in the amount of silica which existed already in the glass marbles packing. This led to longer reaction time required to precipitate silica from the sodium silicate solution and from the large size of the glass marbles packing.

## 4. Optimization

Numerical optimization was performed to reach the optimum conditions of the weight percent of SiO<sub>2</sub>, the weight percent of Na<sub>2</sub>CO<sub>3</sub> and the reaction time responses using Design Expert software. The optimization goals were chosen to reach the maximum %wt of SiO<sub>2</sub> product as represented in Table 7.

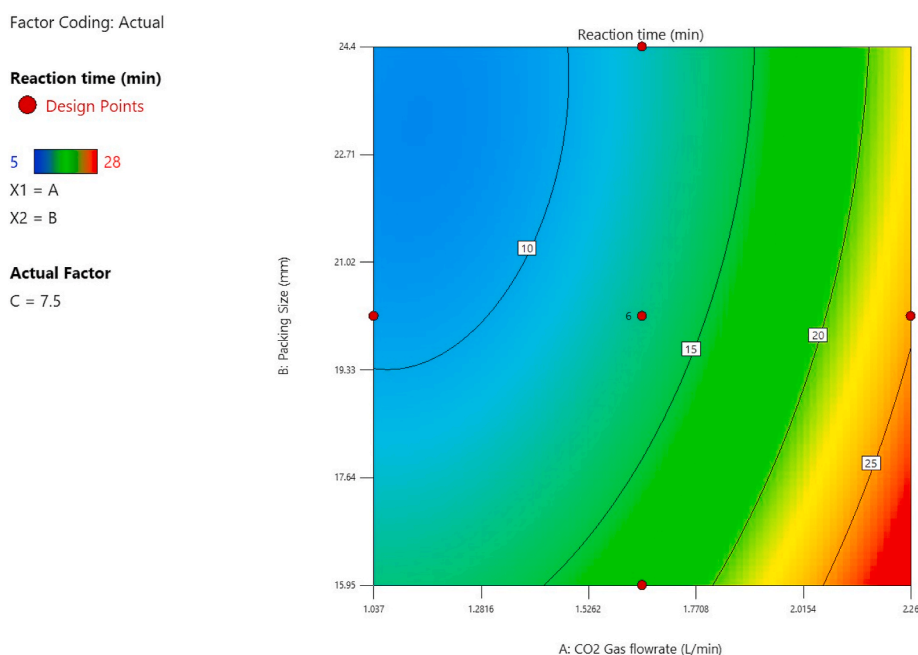


**Fig. 15.** Contour plot of the CO<sub>2</sub> gas flow rate and the packing size versus the reaction time.

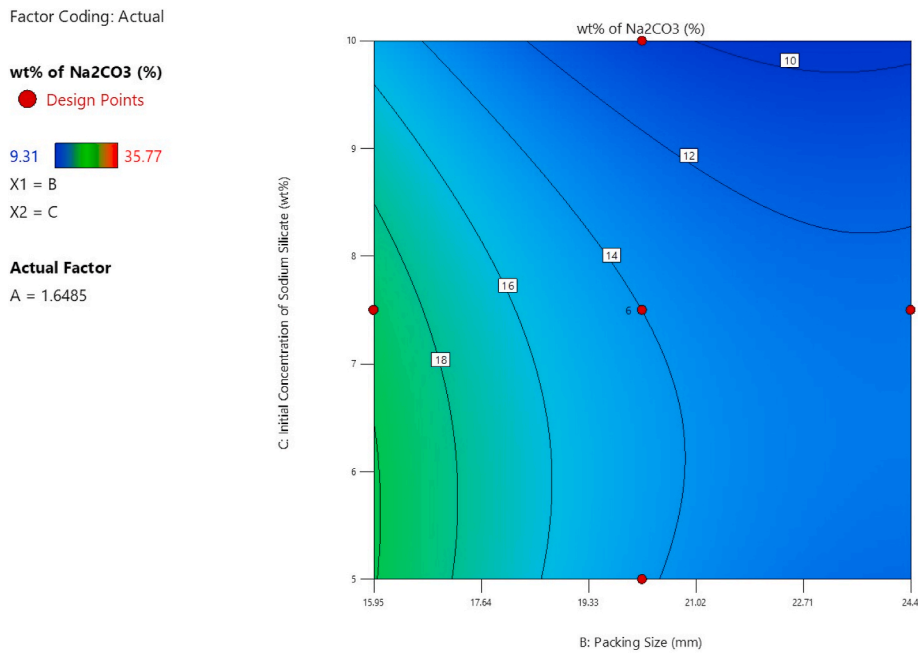


Fig. 16. Contour plot of the packing size and the initial concentration of sodium silicate versus the reaction time.

Fig. 17 a, b and c represented that the optimum levels of %wt of SiO<sub>2</sub>, %wt Na<sub>2</sub>CO<sub>3</sub> and the reaction time were 25.63 %, 9.62 % and 7.59 min, respectively at experimental conditions of initial concentration of sodium silicate solution = 10 %wt, CO<sub>2</sub> gas flow rate = 1.648 L/min and packing size = 24.4 mm.

Fig. 18 illustrated the numerical Pareto graph of desirability by displaying the bar graph. The bar graph is a graphical representation of the optimal solution for each factor. The red bars indicated the optimal factor settings, while the blue bars indicated the optimal response predicted value. According to Fig. 18, the optimal conditions for each factor in terms of desirability are the CO<sub>2</sub> gas flow rate (A/L/min) = 1, packing size (B/mm) (0.9999–1), initial concentration of sodium silicate solution (C/%wt) (0.9999–1), weight percent of SiO<sub>2</sub> (Y1/%wt) (0.9925), weight percent of Na<sub>2</sub>CO<sub>3</sub> (Y2/%wt) (0.9880) and reaction time (Y3/min) (0.8870).

### 5. Preliminary cost effectiveness study

A cost effectiveness study was performed for the designed prototype which used in CO<sub>2</sub> gas absorption using sodium silicate solution. It included the equipment, operating and chemicals costs that were used in this research study. As represented in Tables 8 and 9, the total cost of equipment and energy consumption was \$ 226 and the cost of chemicals was \$180.

Therefore, the overall cost of this research project was \$ 405. The value of the silica produced from this research project was determined and compared with the price of silica in market specially from Sigma Aldrich company in order to estimate the potential benefits of this research. The price of silica produced from this research was calculated as represented in Eqs. (9) and (10);

$$\text{Price of silica} \left( \frac{\$}{\text{kg}} \right) = \frac{\text{overall cost of the research project} (\$)}{\sum \text{weight of silica produced from the research project} (\text{kg})} \tag{9}$$

$$\begin{aligned} \text{Total weight of silica} &= \left( \frac{\% \text{wt of silica of each experiment run}}{100} \right) \\ &\times \sum \text{weight of products of all the experiments runs} (\text{kg}) \end{aligned} \tag{10}$$

Table 7  
Optimization constraints.

Factor	Goal	Lower Limit	Upper Limit	Value
CO <sub>2</sub> gas flow rate (L/min)	target	1.037	2.26	1.6485
Packing size (mm)	Maximize	15.95	24.4	–
Initial concentration of sodium silicate (%wt)	Maximize	5	10	–
%wt of SiO <sub>2</sub>	Maximize	1.52	25.82	–
%wt of Na <sub>2</sub> CO <sub>3</sub>	Minimize	9.31	35.77	–
Reaction time	Minimize	5	28	–

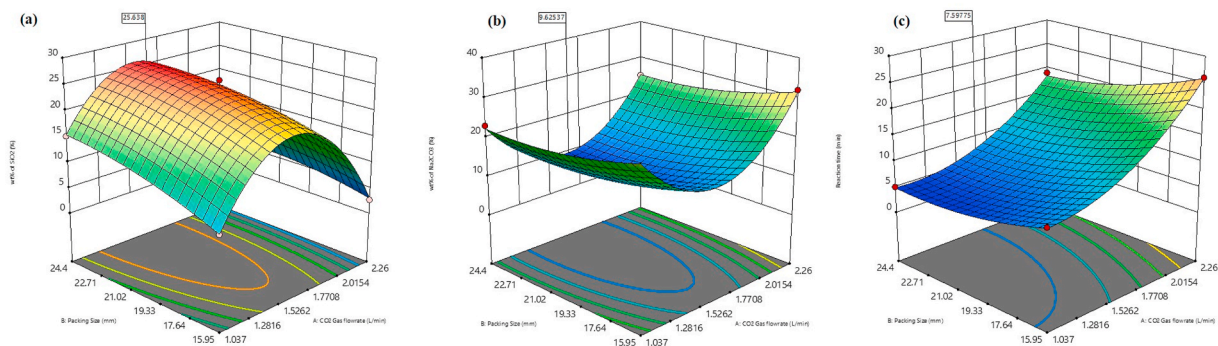


Fig. 17. Response surfaces of the optimum (a) %wt of SiO<sub>2</sub>, (b) %wt Na<sub>2</sub>CO<sub>3</sub> and (c) reaction time, respectively.

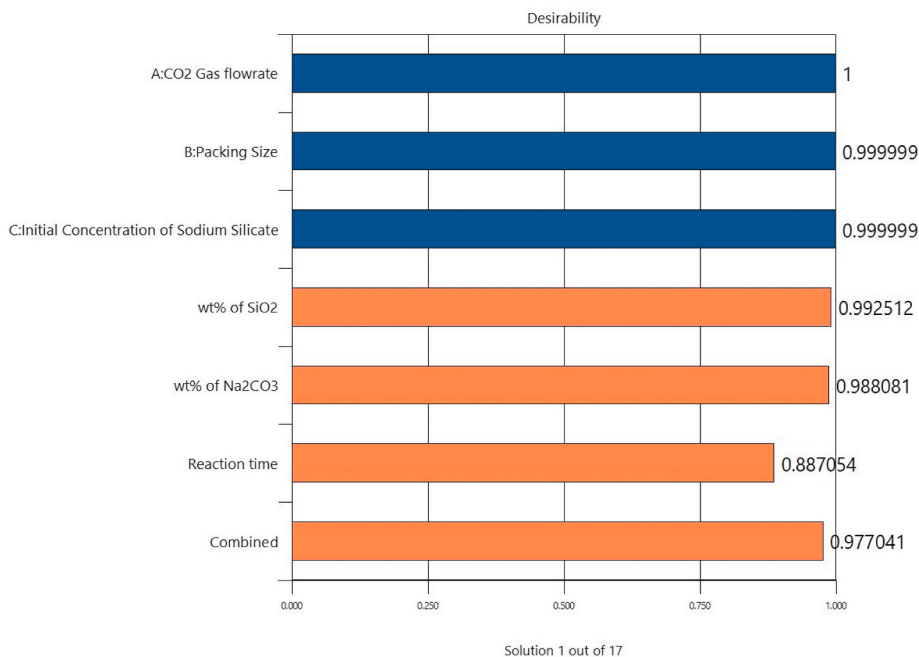


Fig. 18. Numerical optimization bar graph (Pareto graph).

Table 8  
Fixed and operating costs of the research project.

Unit	Cost (\$)
Acrylic	17.5
Carbon steel pipes	8.0
Pressure gauges	17.9
Valves	6.3
pH meter	44.2
Welding, cutting and adhesives	4.2
Packing material (Marbles)	0.4
Pump	29.5
CO <sub>2</sub> feed gas cylinder	6.3
CO <sub>2</sub> gas flowmeter	73.7
Operating cost (electricity & water)	17.9
Total cost	225.9

**Table 9**  
Cost of chemicals used in the research project.

Unit	Cost (\$)
Sodium hydroxide (NaOH) (500 g)	5
Hydrochloric acid (HCl, 36 % v/v) (1L)	14
Ammonium Chloride (NH <sub>4</sub> Cl) (25 gm)	40.89
Silver Nitrate (AgNO <sub>3</sub> ) (1L)	119.7
Total cost	180

Therefore, total weight of silica produced from this research project = 2.37 kg and the total weight of products of all the experiments' runs = 835.7 g = 0.836 kg. The price of silica produced from this research project = \$/kg 171.2 while the price of silica = \$/kg 190.86 ~ €/kg 177. As illustrated the price of silica produced from this research project comparing with its market price ensured that this project has proven its efficiency and applicability.

## 6. Conclusion

Carbon dioxide (CO<sub>2</sub>) is one of the most damaging and pervasive greenhouse gas, and its increasing anthropogenic emission into the atmosphere is causing global warming. Therefore, in this study, a designed apparatus has been used to convert carbon dioxide gas into silica via a chemical absorption process using a green absorbent (sodium silicate) extracted from sugarcane bagasse.

Surface characterization of the sodium silicate extracted from sugarcane bagasse and products from the CO<sub>2</sub> absorption process in the designed apparatus were performed including Scanning Electron Microscopy (SEM) and Fourier Transform Infrared Spectroscopy (FTIR) to illustrate the surface morphology and the weight percents of the products.

In this study, a wide range of experimental parameters were investigated, including the flow rate of CO<sub>2</sub> gas (1.037, 1.648, and 2.26 L/min), the initial concentration of sodium silicate solution (5 %, 7.5 %, and 10 % by weight), as well as the packing size (24.4, 20.175, and 15.95 mm) to assess their impact on silica and sodium carbonate production and reaction time.

Optimum conditions of the experiments for maximizing the weight percent of SiO<sub>2</sub> (primary product), minimizing the weight percent of Na<sub>2</sub>CO<sub>3</sub> (side product), and shortening the reaction time were achieved via the assistance of the Design Expert software program. The optimum conditions obtained were the CO<sub>2</sub> gas flow rate of 1.648 L/min, the packing size of 24.4 mm, and the sodium silicate solution concentration of 10 % by weight. Applying the above-mentioned optimal conditions resulted in the highest percent of SiO<sub>2</sub> (25.638 %), the lowest percent of Na<sub>2</sub>CO<sub>3</sub> (9.62 %), and the shortest reaction time (7.59 min).

## Future research

There are several potential avenues for future work in chemical absorption of CO<sub>2</sub> gas using sodium silicate solution. Here are a few possibilities:

- Scale-up and commercialization: Once the process has been optimized, there is potential for scale-up and commercialization of the technology. This will involve working with industry partners to develop large-scale systems for CO<sub>2</sub> capture.
- Environmental impact assessment: Environmental impact of the process will be explored, including the energy required for the process, the carbon footprint of the materials used, and the potential for waste disposal issues. This could help to ensure that the process is sustainable and environmentally friendly.

## Data availability

The data used to support this study's findings are available from the corresponding author upon request. Data included in this article are referenced in this article.

## CRediT authorship contribution statement

**Dalia Amer Ali:** Writing – review & editing, Writing – original draft, Validation, Supervision, Software, Resources, Methodology, Formal analysis. **Mohamed Essam Ibrahim:** Writing – original draft, Software, Resources.

## Declaration of competing interest

The authors declare the following financial interests/personal relationships which may be considered as potential competing interests: Dalia Amer Ahmed Ali reports article publishing charges was provided by The British University in Egypt. Dalia Amer Ahmed Ali reports a relationship with The British University in Egypt that includes: employment. If there are other authors, they declare that they have no known competing financial interests or personal relationships that could have appeared to influence the work reported in this paper.

## Acknowledgments

The authors are thankful to the British University in Egypt (BUE), Cairo, Egypt for providing the article publishing charges and the necessary facilities to carry out this work.

## References

- [1] C.K. Lau, G. Gozgor, M.K. Mahalik, G. Patel, J. Li, Introducing a new measure of energy transition: green quality of energy mix and its impact on CO<sub>2</sub> emissions, *Energy Econ.* 122 (April) (2023) 106702, <https://doi.org/10.1016/j.eneco.2023.106702>.
- [2] C. Wang, Z. Wang, X. Leng, Simulation and comprehensive study of an optimum process for CO<sub>2</sub> capture from flue gas; technical, economic, and environmental analyses, *Alex. Eng. J.* 74 (2023) 121–138, <https://doi.org/10.1016/j.aej.2023.04.066>.
- [3] P. Madejski, K. Chmiel, N. Subramanian, T. Kus, Methods and techniques for CO<sub>2</sub> capture : review of potential, *Energies* 15 (2022) 887.
- [4] J. Wu, Y. Huang, W. Ye, Y. Li, CO<sub>2</sub> reduction: from the electrochemical to photochemical approach, *Adv. Sci.* 4 (11) (2017) 1–29, <https://doi.org/10.1002/advs.201700194>.
- [5] F. Khosroabadi, A. Aslani, K. Bekhrad, Z. Zolfaghari, Analysis of carbon dioxide capturing technologies and their technology developments, *Clean. Eng. Technol.* 5 (September) (2021) 100279, <https://doi.org/10.1016/j.clet.2021.100279>.
- [6] S. Vaz, A.P. Rodrigues de Souza, B.E. Lobo Baeta, Technologies for carbon dioxide capture: a review applied to energy sectors, *Clean. Eng. Technol.* 8 (February) (2022) 100456, <https://doi.org/10.1016/j.clet.2022.100456>.
- [7] X.L. Yue, Q.X. Gao, Contributions of natural systems and human activity to greenhouse gas emissions, *Adv. Clim. Change Res.* 9 (4) (2018) 243–252, <https://doi.org/10.1016/j.accre.2018.12.003>.
- [8] United States Department of State, The long-term strategy of the United States: pathways to net-zero greenhouse gas emissions by 2050, *leee* (November) (2021) 1–63 [Online]. Available: <https://www.whitehouse.gov/wp-content/uploads/2021/10/US-Long-Term-Strategy.pdf>.
- [9] J.I. Mikayilov, M. Galeotti, F.J. Hasanov, The impact of economic growth on CO<sub>2</sub> emissions in Azerbaijan, *J. Clean. Prod.* 197 (2018) 1558–1572, <https://doi.org/10.1016/j.jclepro.2018.06.269>.
- [10] S. Kammerer, I. Borho, J. Jung, M.S. Schmidt, Review: CO<sub>2</sub> capturing methods of the last two decades, *Int. J. Environ. Sci. Technol.* 20 (7) (2023) 8087–8104, <https://doi.org/10.1007/s13762-022-04680-0>.
- [11] L. Fu, et al., Research progress on CO<sub>2</sub> capture and utilization technology, *J. CO<sub>2</sub> Util.* 66 (July) (2022) 102260, <https://doi.org/10.1016/j.jcou.2022.102260>.
- [12] A.I. Osman, M. Hefny, M.I.A. Abdel Maksoud, A.M. Elgarahy, D.W. Rooney, Recent advances in carbon capture storage and utilisation technologies: a review, *Springer International Publishing* 19 (2) (2021), <https://doi.org/10.1007/s10311-020-01133-3>.
- [13] U. Khan, et al., Assessing absorption-based CO<sub>2</sub> capture: research progress and techno-economic assessment overview, *Carbon Capture Sci. Technol.* 8 (May) (2023) 100125, <https://doi.org/10.1016/j.ccs.2023.100125>.
- [14] N.S. Sifat, Y. Haseli, A critical review of CO<sub>2</sub> capture technologies and prospects for clean power generation, *Energies* 12 (21) (2019), <https://doi.org/10.3390/en12214143>.
- [15] H. Ababneh, A. AlNouss, I.A. Karimi, S.A. Al-Muhtaseb, Natural gas sweetening using an energy-efficient, state-of-the-art, solid–vapor separation process, *Energies* 15 (14) (2022) 1–12, <https://doi.org/10.3390/en15145286>.
- [16] G. Ji, M. Zhao, Membrane separation technology in carbon capture, *Recent Adv. Carbon Capture Storage* (March) (2017), <https://doi.org/10.5772/65723>.
- [17] C.M. Quintella, S.A. Hatimondi, A.P.S. Musse, S.F. Miyazaki, G.S. Cerqueira, A. De Araujo Moreira, CO<sub>2</sub> capture technologies: an overview with technology assessment based on patents and articles, *Energy Proc.* 4 (2011) 2050–2057, <https://doi.org/10.1016/j.egypro.2011.02.087>.
- [18] M. Leimbrink, T. Limberg, A.K. Kunze, M. Skiborowski, Different strategies for accelerated CO<sub>2</sub> absorption in packed columns by application of the biocatalyst carbonic anhydrase, *Energy Proc.* 114 (November 2016) (2017) 781–794, <https://doi.org/10.1016/j.egypro.2017.03.1221>.
- [19] M. Yusuf, Selection of amine in natural gas sweetening process for acid gases removal: a review of recent studies, *Pet. Petrochemical Eng. J.* 1 (2) (2017), <https://doi.org/10.23880/ppej-16000114>.
- [20] H. Rashidi, R. Sohrabi, Detailed performance model of carbon dioxide absorption utilizing titanium dioxide nanoparticles in a wetted wall column, *Environ. Prog. Sustain. Energy* 38 (6) (2019) 1–10, <https://doi.org/10.1002/ep.13211>.
- [21] A. Hemmati, H. Rashidi, Optimization of industrial intercooled post-combustion CO<sub>2</sub> absorber by applying rate- base model and response surface methodology (RSM), *Process Saf. Environ. Protect.* 121 (2019) 77–86, <https://doi.org/10.1016/j.psep.2018.10.009>.
- [22] Jack T. Ballinger, Gershon J. Shugar, “GRAVIMETRIC analysis.”, in: Chap. 15 in *Chemical Technicians’ Ready Reference Handbook*, fifth ed., McGraw-Hill, New York, 2011.
- [23] P. Chindaprasirt, U. Rattanasak, Eco-production of silica from sugarcane bagasse ash for use as a photochromic pigment filler, *Sci. Rep.* 10 (1) (2020) 1–9, <https://doi.org/10.1038/s41598-020-66885-y>.
- [24] I. Works, Part I 蛋白质的翻译后修饰简介 Part I 蛋白质的翻译后修饰简介, *Instruments L. Policy Deal. with Scarcity L 1* (2018) 1–27, no. August.
- [25] P.M. Mathias, S. Reddy, A. Smith, K. Afshar, A guide to evaluate solvents and processes for post-combustion CO<sub>2</sub> capture, *Energy Proc.* 37 (December 2013) (2013) 1863–1870, <https://doi.org/10.1016/j.egypro.2013.06.066>.
- [26] J. Xia, S. Liu, B. Zhang, Y. Chen, Central Composite Experiment Design (CCD) -Response, Ccd, 2021.
- [27] A. Asghar, A.A.A. Raman, W.M.A.W. Daud, A comparison of central composite design and taguchi method for optimizing Fenton process, *Sci. World J.* 2014 (2014), <https://doi.org/10.1155/2014/869120>.
- [28] D.F. Maki, A.S. Yasiry, H.A.K. Shahad, Optimization of performance and emission responses for a CIE run by meoh/biodiesel/diesel blends utilizing response surface methodology, *IOP Conf. Ser. Mater. Sci. Eng.* 1094 (1) (2021) 012121, <https://doi.org/10.1088/1757-899x/1094/1/012121>.
- [29] J. Zhu, et al., Effect of Na<sub>2</sub>CO<sub>3</sub> on the microstructure and macroscopic properties and mechanism analysis of PVA/CMC composite film, *Polymers* 12 (2) (2020) 1–13, <https://doi.org/10.3390/polym12020453>.
- [30] X. Cai, et al., Synthesis of silica powders by pressured carbonation, *Chem. Eng. J.* 151 (1–3) (2009) 380–386, <https://doi.org/10.1016/j.cej.2009.03.060>.
- [31] H.Y. Nah, et al., Role of oxalic acid in structural formation of sodium silicate-based silica aerogel by ambient pressure drying, *J. Sol. Gel Sci. Technol.* 85 (2) (2018) 302–310, <https://doi.org/10.1007/s10971-017-4553-2>.
- [32] S. Saravanan, R.S. Dubey, Synthesis of SiO<sub>2</sub>nanoparticles by sol-gel method and their optical and structural properties, *Rom. J. Inf. Sci. Technol.* 23 (1) (2020) 105–112.
- [33] B.H. Stuart, *Infrared Spectroscopy: Fundamentals and Applications*, vol. 8, 2005, <https://doi.org/10.1002/0470011149>.
- [34] N. Sahiron, N. Rahmat, F. Hamzah, Pencirian natrium silikat yang dihasilkan daripada abu hampas tebu, *Malaysian J. Anal. Sci.* 21 (2) (2017) 512–517, <https://doi.org/10.17576/mjas-2017-2102-26>.